# Polyakov loop, diquarks and the two-flavour phase diagram *

S. Rößner[a], C. Ratti[b] and W. Weise[a]

[a] Physik-Department, Technische Universität München, D-85747 Garching, Germany

[b] ECT*, I-38050 Villazzano (Trento) Italy and INFN, Gruppo Collegato di Trento, via Sommarive, I-38050 Povo (Trento) Italy

September 27, 2006

**Abstract**

An updated version of the PNJL model is used to study the thermodynamics of $N_f = 2$ quark flavors interacting through chiral four-point couplings and propagating in a homogeneous Polyakov loop background. Previous PNJL calculations are extended by introducing explicit diquark degrees of freedom and an improved effective potential for the Polyakov loop field. The input is fixed exclusively by selected pure-gauge lattice QCD results and by pion properties in vacuum. The resulting $(T, \mu)$ phase diagram is studied with special emphasis on the critical point, its dependence on the quark mass and on Polyakov loop dynamics. We present successful comparisons with lattice QCD thermodynamics expanded to finite chemical potential $\mu$.

## 1 Introduction

Reconstructing the phase diagram and thermodynamics of QCD in terms of field theoretical quasiparticle models is an effort worth pursuing in order to interpret lattice QCD results [1–7] and extrapolate into regions not accessible by lattice computations. A promising ansatz of this sort is the PNJL model [9–12], a synthesis of Polyakov loop dynamics with the Nambu & Jona-Lasinio model, combining the two principal non-perturbative features of low-energy QCD: confinement and spontaneous chiral symmetry breaking. This paper extends our previous PNJL calculations

*Work supported in part by BMBF, GSI and INFN

[11] in several directions. First, diquark degrees of freedom are explicitly included. Diquark condensation at large quark chemical potential is explored in the presence of a Polyakov loop background. Secondly, in comparison with our previous work, the effective potential which controls the thermodynamics of the Polyakov loop field is improved such that group theoretical constraints are rigorously implemented, following Ref.[9]. The aim of the present paper is to investigate the phase diagram resulting from this approach. Of special interest is the location of the critical point, its dependence on the quark mass and the role of the Polyakov loop as indicator of the deconfinement transition. Predictions for the leading coefficients in a Taylor expansion of the pressure in powers of the quark chemical potential will turn out to be remarkably successful in comparison with corresponding lattice QCD results.

# 2 The PNJL model

The two-flavor PNJL model (now including diquark degrees of freedom) is specified by the Euclidean action

$$\mathcal{S}_E(\psi,\psi^\dagger,\phi) = \int_0^{\beta=1/T} d\tau \int d^3x \left[\psi^\dagger\,\partial_\tau\,\psi + \mathcal{H}(\psi,\psi^\dagger,\phi)\right] + \delta\mathcal{S}_E(\phi,T) \qquad (1)$$

with the fermionic Hamiltonian density [1]:

$$\mathcal{H} = -i\psi^\dagger\left(\vec{\alpha}\cdot\vec{\nabla} + \gamma_4\, m_0 - \phi\right)\psi + \mathcal{V}(\psi,\psi^\dagger)\ , \qquad (2)$$

where $\psi$ is the $N_f = 2$ doublet quark field and $m_0 = diag(m_u, m_d)$ is the quark mass matrix. The quarks move in a background color gauge field $\phi \equiv A_4 = iA_0$, where $A_0 = \delta_{\mu 0}\, g\mathcal{A}^\mu_a\, t^a$ with the $SU(3)_c$ gauge fields $\mathcal{A}^\mu_a$ and the generators $t^a = \lambda^a/2$. The matrix valued, constant field $\phi$ relates to the (traced) Polyakov loop as follows:

$$\Phi = \frac{1}{N_c}\mathrm{Tr}\left[\mathcal{P}\exp\left(i\int_0^\beta d\tau A_4\right)\right] = \frac{1}{3}\mathrm{Tr}\, e^{i\phi/T}\ , \qquad (3)$$

In a convenient gauge (the so-called Polyakov gauge), the matrix $\phi$ is given a diagonal representation

$$\phi = \phi_3\,\lambda_3 + \phi_8\,\lambda_8\ , \qquad (4)$$

which leaves only two independent variables, $\phi_3$ and $\phi_8$. The piece $\delta\mathcal{S}_E = -\frac{V}{T}\mathcal{U}$ of the action (1) controls the thermodynamics of the Polyakov loop. It will be specified later in terms of the effective potential, $\mathcal{U}(\Phi,T)$, determined such that the thermodynamics of pure gauge lattice QCD is reproduced for $T$ up to about twice the critical temperature for deconfinement. At much higher temperatures

[1] $\vec{\alpha} = \gamma_0\,\vec{\gamma}$ and $\gamma_4 = i\gamma_0$ in terms of the standard Dirac $\gamma$ matrices.

where transverse gluons begin to dominate, the PNJL model is not supposed to be applicable.

The interaction $\mathcal{V}$ in Eq. (2) includes chiral $SU(2) \times SU(2)$ invariant four-point couplings of the quarks acting in pseudoscalar-isovector/scalar-isoscalar quark-antiquark and scalar diquark channels:

$$\mathcal{V} = -\frac{G}{2}\left[\left(\bar{\psi}\psi\right)^2 + \left(\bar{\psi}\, i\gamma_5 \vec{\tau}\, \psi\right)^2\right] - \frac{H}{2}\left[\left(\bar{\psi}\, \mathcal{C}\gamma_5\tau_2\lambda_2\, \bar{\psi}^T\right)\left(\psi^T \gamma_5\tau_2\lambda_2 \mathcal{C}\, \psi\right)\right] \ , \qquad (5)$$

where $\mathcal{C}$ is the charge conjugation operator. We can think of Eq.(5) as a subset in the chain of terms generated by Fierz-transforming a local color current-current interaction between quarks,

$$\mathcal{L}_{int} = -G_c(\bar{\psi}\gamma_\mu t^a \psi)(\bar{\psi}\gamma^\mu t^a \psi) \ .$$

In this case the coupling strengths in the quark-antiquark and diquark sectors are related by $G = \frac{4}{3}H$, the choice we adopt. The minimal ansatz (5) for $\mathcal{V}$ is motivated by the fact that spontaneous chiral symmetry breaking is driven by the first term while the second term induces diquark condensation at sufficiently large chemical potential of the quarks. Additional pieces representing vector and axialvector $q\bar{q}$ excitations as well as color-octet diquark and $q\bar{q}$ modes are omitted here. We have checked that their effects are not important in the present context.

The NJL part of the model involves three parameters: the quark mass which we take equal for $u$- and $d$-quarks, the coupling strength $G$ and a three-momentum cutoff $\Lambda$. We take those from Ref.[11]:

$$m_{u,d} = 5.5 \text{ MeV} \ , \quad G = \frac{4}{3}H = 10.1 \text{ GeV}^{-2} \ , \quad \Lambda = 0.65 \text{ GeV} \ ,$$

which were fixed to reproduce the pion mass and decay constant in vacuum and the chiral condensate as $m_\pi = 139.3$ MeV, $f_\pi = 92.3$ MeV and $\langle\bar{\psi}_u\psi_u\rangle = -(251 \text{ MeV})^3$.

The effective potential $\mathcal{U}(\Phi, T)$ which controls the dynamics of the Polyakov loop has the following properties. It must satisfy the $Z(3)$ center symmetry of the pure gauge QCD Lagrangian. In the low-temperature (confinement) phase $\mathcal{U}(\Phi)$ has an absolute minimum at $\Phi = 0$. Above the critical temperature for deconfinement ($T_0 \simeq 270$ MeV according to pure gauge lattice QCD results) the $Z(3)$ symmetry is spontaneously broken and the minimum of $\mathcal{U}(\Phi)$ is shifted to a finite value of $\Phi$. In the limit $T \to \infty$ we have $\Phi \to 1$.

In our previous Ref.[11] the simplest possible polynomial form was chosen for $\mathcal{U}$. In the present work an improved expression, guided by Ref.[9], replaces the higher order polynomial terms in $\Phi, \Phi^*$ by the logarithm of $J(\Phi)$, the Jacobi determinant which results from integrating out six non-diagonal group elements while keeping the two diagonal ones, $\phi_{3,8}$, to represent $\Phi$. This suggests the following ansatz for

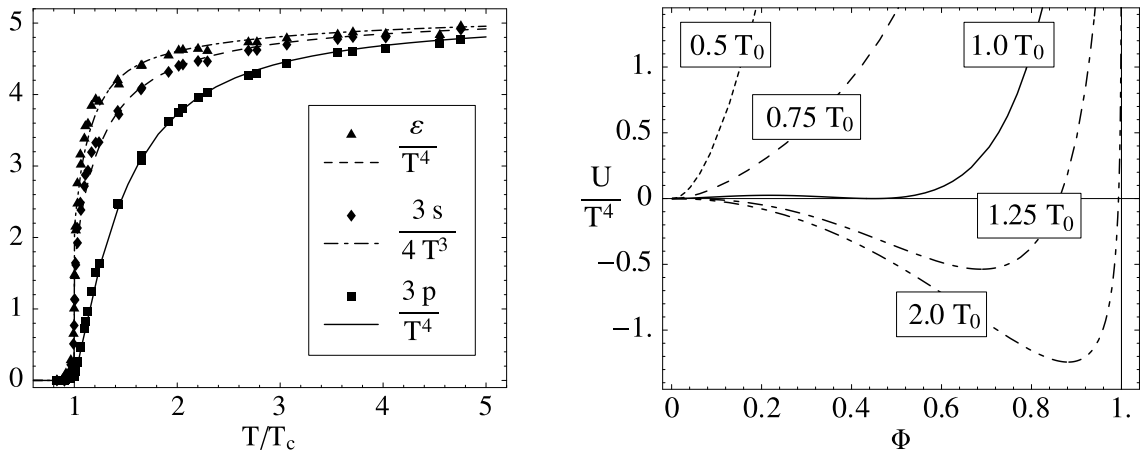


Figure 1: Left: Fit to scaled pressure, entropy density and energy density as functions of the temperature in the pure gauge sector, compared to the corresponding lattice data taken from Ref. [5]. Right: Resulting effective potential (6) that drives spontaneous Z(3) symmetry breakdown at $T = T_0$.

$\mathcal{U}$:

$$\mathcal{U}(\Phi, T) = -\frac{1}{2}a(T)\,\Phi^*\Phi + b(T)\,\ln\left[1 - 6\,\Phi^*\Phi + 4\left(\Phi^{*3} + \Phi^3\right) - 3\,(\Phi^*\Phi)^2\right] \qquad (6)$$

with

$$a(T) = a_0 + a_1\left(\frac{T_0}{T}\right) + a_2\left(\frac{T_0}{T}\right)^2, \qquad b(T) = b_3\left(\frac{T_0}{T}\right)^3. \qquad (7)$$

With its logarithmic divergence as $\Phi, \Phi^* \to 1$, this ansatz automatically limits the Polyakov loop $\Phi$ to be always smaller than 1, reaching this value asymptotically only as $T \to \infty$. Following the procedure as in [11], a precision fit of the parameters $a_i$ and $b_3$ is performed in order to reproduce lattice data for pure gauge QCD thermodynamics and for the behaviour of the Polyakov loop as a function of temperature. The results of this combined fit are shown in Figs 1 and 2 (dotted line). The corresponding parameters are

$$a_0 = 3.51\ , \quad a_1 = -2.47\ , \quad a_2 = 15.22\ , \quad b_3 = -1.75\ .$$

The critical temperature $T_0$ for deconfinement in the pure gauge sector is fixed at 270 MeV in agreement with lattice results.

Next, the PNJL action is bosonized and rewritten in terms of the auxiliary scalar and pseudoscalar fields $(\sigma, \vec{\pi})$, and diquark fields $(\Delta, \Delta^*)$. The thermodynamic potential of the model is evaluated as follows:

$$\Omega = \mathcal{U}\left(\Phi, T\right) - \frac{T}{2}\sum_n \int \frac{d^3p}{(2\pi)^3}\mathrm{Tr}\ln\left[\beta\tilde{S}^{-1}\left(i\omega_n, \vec{p}\right)\right] + \frac{\sigma^2}{2G} + \frac{\Delta^*\Delta}{2H}\ , \qquad (8)$$

where the sum is taken over Matsubara frequencies $\omega_n = (2n+1)\pi T$. The inverse Nambu-Gor'kov propagator including diquarks is:

$$\tilde{S}^{-1}(i\omega_n, \vec{p}) = \begin{pmatrix} i\gamma_0\,\omega_n - \vec{\gamma}\cdot\vec{p} - m + \gamma_0\,(\mu - i\phi) & \Delta\gamma_5\tau_2\lambda_2 \\ -\Delta^*\gamma_5\tau_2\lambda_2 & i\gamma_0\,\omega_n - \vec{\gamma}\cdot\vec{p} - m - \gamma_0\,(\mu - i\phi) \end{pmatrix}, \tag{9}$$

Just as in the standard NJL model, quarks develop a dynamical (constituent) mass through their interaction with the chiral condensate:

$$m = m_0 - \langle\sigma\rangle = m_0 - G\langle\bar{\psi}\psi\rangle. \tag{10}$$

With the input parameters previously specified one finds $m = 325$ MeV at $T = 0$.

Note that introducing diquarks (and anti-diquarks) as explicit degrees of freedom implies off-diagonal pieces in the inverse propagator (9). As a consequence, the traced Polyakov loop field $\Phi$ and its conjugate $\Phi^*$ can no longer be factored out when performing the Tr ln = ln det operation in the thermodynamic potential (8), unlike the simpler case treated in our previous Ref. [11]. The explicit evaluation of energy eigenvalues now involves $\phi_3$ and $\phi_8$ as independent fields. The final result for $\Omega$ is then given as:

$$\begin{aligned} \Omega &= \mathcal{U}(\Phi, T) + \frac{\sigma^2}{2G} + \frac{\Delta^*\Delta}{2H} \\ &- 2N_f \int \frac{d^3p}{(2\pi)^3} \sum_j \left\{ T \ln\left[1 + e^{-E_j/T}\right] + \frac{1}{2}\Delta E_j \right\} . \end{aligned} \tag{11}$$

The quasi-particle energies $E_j$, denoted by indices $j$ running from 1 to 6, have the following explicit expressions with $\varepsilon(\vec{p}) = \sqrt{\vec{p}^{\,2} + m^2}$:

$$\begin{aligned} E_{1,2} &= \varepsilon(\vec{p}) \pm \tilde{\mu}_b \ , \\ E_{3,4} &= \sqrt{(\varepsilon(\vec{p}) + \tilde{\mu}_r)^2 + |\Delta|^2} \pm i\,\phi_3 \ , \\ E_{5,6} &= \sqrt{(\varepsilon(\vec{p}) - \tilde{\mu}_r)^2 + |\Delta|^2} \pm i\,\phi_3 \ , \end{aligned} \tag{12}$$

with

$$\tilde{\mu}_b = \mu + 2i\,\frac{\phi_8}{\sqrt{3}} \ , \qquad \tilde{\mu}_r = \mu - i\,\frac{\phi_8}{\sqrt{3}} \ . \tag{13}$$

In Eq.(11), $\Delta E_j = E_j - \varepsilon \pm \mu$ is the difference of the quasiparticle energy $E_j$ and the energy of free fermions (quarks), where the lower sign applies for fermions and the upper sign for antifermions. It is understood that for three-momenta $|\vec{p}|$ above the cutoff $\Lambda$ where NJL interactions are "turned off", the quantities $\sigma$ and $\Delta, \Delta^*$ are set to zero.

In general, the Euclidean action $\mathcal{S}_E$ is formally complex in the presence of the temporal gauge field $\phi$. It is real only at vanishing chemical potential, $\mu = 0$. In this limiting case charge conjugation symmetry implies that the action, taken as the sum of $\mathcal{S}_E$ and its charge conjugate, is real [13]. This is no longer true for non-vanishing chemical potential. In this case one has, in addition, $\langle\Phi\rangle \neq \langle\Phi^*\rangle$.

The field configuration that contributes most importantly to the path integral is the one which minimizes the real part of the Euclidean action or, equivalently, the real part of the thermodynamic potential. The mean field equations derived from $\Omega$ are therefore of the form

$$\frac{\partial\,\mathrm{Re}\,\Omega}{\partial\varphi} = 0 \tag{14}$$

with $\varphi = \sigma, \Delta, \phi_3, \phi_8$. At this mean field level, the additional constraint of $\phi_i$ being real implies that the action is minimized by $\phi_8 = 0$. It follows that $\Phi \sim \mathrm{Tr}\exp(i\lambda_3\,\phi_3/T)$ is real (i.e. $\Phi = \Phi^*$). Fluctuations beyond mean field are at the origin of $\langle\Phi\rangle \neq \langle\Phi^*\rangle$ for $\mu \neq 0$. This paper deals with self-consistent solutions and predictions of the mean-field equations (14). While further extensions including quantum fluctuations [14] will be subject of a forthcoming presentation [15], we can already anticipate one of the results, namely that the effects of fluctuations, leading to $\langle\Phi\rangle \neq \langle\Phi^*\rangle$ at finite chemical potential, turn out not to be of major qualitative importance in determining the phase diagram.

# 3 Results

Solution of the mean-field equations (14) yields the chiral condensate, $\langle\bar\psi\psi\rangle = \sigma/G$, the color-antitriplet diquark condensate, $\Delta$, and the Polyakov loop exponent $\phi_3$ as functions of $T, \mu$. The resulting prediction for the traced Polyakov loop $\Phi$ is shown in Fig. 2 (continuous line) in comparison with the corresponding lattice data taken from Ref. [7] (full symbols). The agreement is quite remarkable. In the presence of quarks, the deconfinement transition is no longer first order as in pure gauge QCD. It becomes a smooth crossover when quarks couple to the Polyakov loop field. The critical temperature for deconfinement is now decreased from 270 MeV to a smaller value around 215 MeV [2] (not evident from Fig. 2 where the results are plotted as functions of $T/T_c$). In Fig. 3 we show in addition the predicted temperature dependence of the two-flavour chiral condensate $\langle\bar\psi\psi\rangle$ in comparison with lattice data [8].

[2] Note that the critical temperature in full lattice QCD reported in [7] is $T_c = 202\,\mathrm{MeV}$.

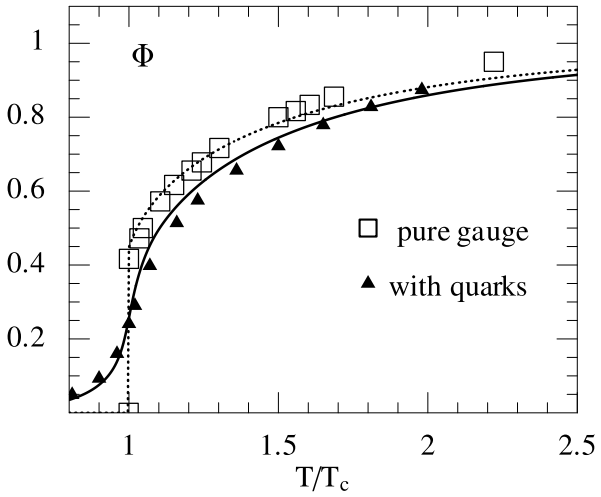


Figure 2: Using the fit of the Polyakov loop (dotted line) to lattice results taken from Ref. [6] in the pure gauge sector (empty symbols), the PNJL model predicts the Polyakov loop behaviour as a function of temperature in the presence of dynamical quarks (solid line). This prediction is compared lattice data in two flavours (full symbols) taken from Ref. [7].

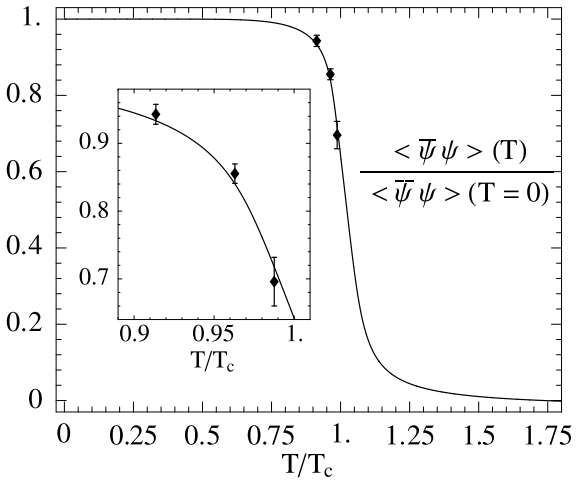


Figure 3: The spontaneous chiral symmetry breaking mechanism of the PNJL model generates a temperature dependent chiral condensate $\langle\bar{\psi}\psi\rangle$ (solid line), which is compared here to lattice QCD results, with selected (two-flavour) data taken from Ref. [8].

## 3.1 Finite chemical potential

Lattice results at finite quark chemical potential are obtained as Taylor expansions of the thermodynamical quantities in the parameter $\mu/T$ around zero chemical potential. Here we perform the same kind of expansion in the PNJL model and compare with Taylor coefficients deduced from lattice data. Examples are the coefficients in the expansion of the pressure $p = -\Omega$:

$$\frac{p(T,\mu)}{T^4} = \sum_{n=0}^{\infty} c_n(T) \left(\frac{\mu}{T}\right)^n \qquad \text{with} \qquad c_n(T) = \frac{1}{n!} \frac{\partial(p(T,\mu)/T^4)}{\partial(\mu/T)^n}\bigg|_{\mu=0} \tag{15}$$

and even $n$. Specifically:

$$\begin{aligned} c_2 &= \frac{1}{2} \frac{\partial^2(p/T^4)}{\partial(\mu/T)^2}\bigg|_{\mu=0}, & c_4 &= \frac{1}{24} \frac{\partial^4(p/T^4)}{\partial(\mu/T)^4}\bigg|_{\mu=0}, \\ c_6 &= \frac{1}{720} \frac{\partial^6(p/T^4)}{\partial(\mu/T)^6}\bigg|_{\mu=0}, & c_8 &= \frac{1}{40320} \frac{\partial^8(p/T^4)}{\partial(\mu/T)^8}\bigg|_{\mu=0}. \end{aligned} \tag{16}$$

Results for these coefficients are shown in Fig. 4. We notice in particular the remarkably good agreement between the calculated "susceptibility" $c_4$ and the lattice data. This quantity has recently been computed in Ref. [16] using the previous version of our PNJL model, Ref. [11], with a less satisfactory outcome. Now, with the improved effective potential $\mathcal{U}$ as described in Eq.(6), the agreement is significantly better.

## 3.2 Phase diagram

We now turn to the phase diagram in the $(T, \mu)$ plane as derived from this updated version of the PNJL model. The left panel of Fig. 5 shows the phase diagrams in the $(T, \mu)$-plane computed using the PNJL model in comparison with the NJL model (the limiting case in which $\Phi \equiv 1$). Of particular interest is the location of the critical endpoint at which the chiral and deconfinement crossover transitions at lower $\mu$ turn into a first-order phase transition above some critical $\mu$. The crossover is not a phase transition. Therefore there exist several ways to locate the position of a crossover transition. In the present calculations the crossover line is determined using the order parameters in the chiral limit (the chiral condensate) and the pure gauge theory (the Polyakov loop) respectively. Since these order parameters show their strongest changes as functions of temperature along the crossover transition lines, we determine their position by local maxima of $\mathrm{d}\sigma/\mathrm{d}T$ and $\mathrm{d}\Phi/\mathrm{d}T$ [3].

[3] Other frequently used and closely related criteria for the definition of crossover transition lines involve chiral or Polyakov loop susceptibilities. This does not lead to any significant differences for the phase diagram in comparison with the method applied here.

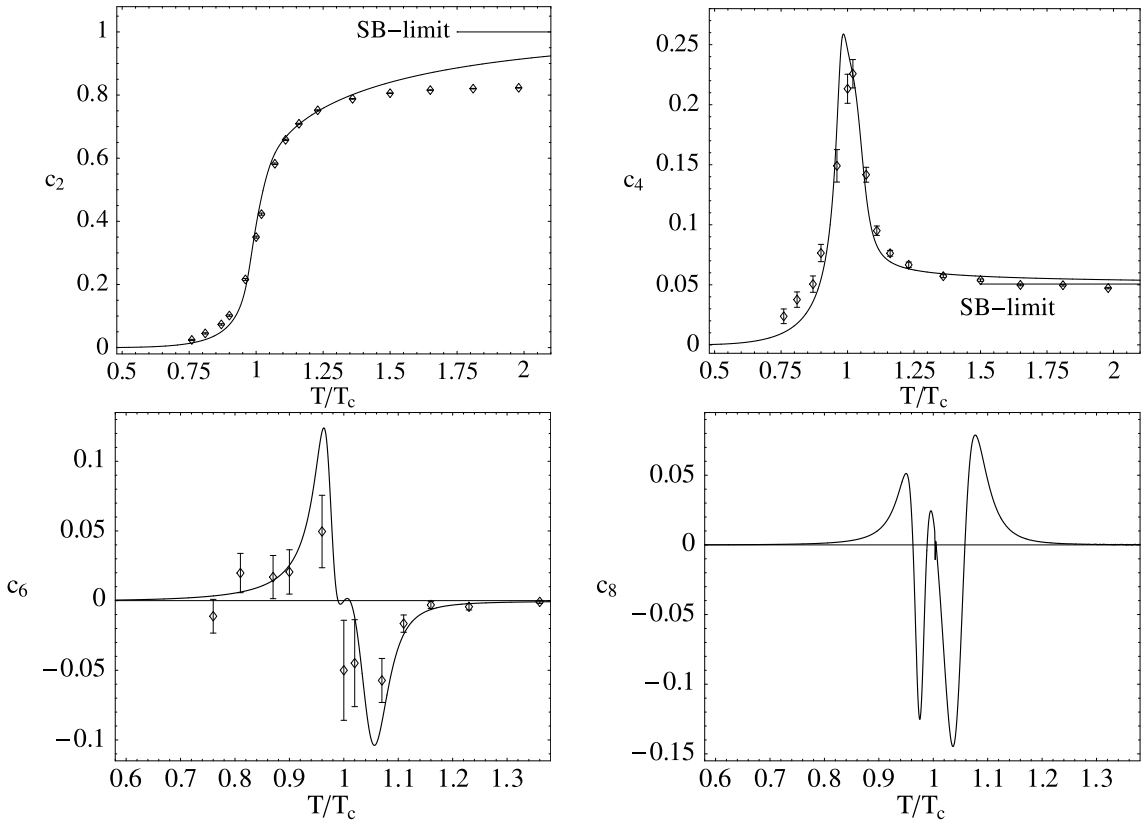


Figure 4: Second, fourth, sixth and eighth moment of the pressure difference with respect to the chemical potential, plotted as functions of the temperature. (Note that the temperature scales of the upper and lower graphs are different.) We compare to lattice data (diamonds with errorbars) taken from Ref. [4]

The crossover transition lines fixed by either the susceptibilities of $\sigma$ and $\Phi$ or by maximal changes with temperature, i.e. zeros of $\mathrm{d}^2\sigma/\mathrm{d}T^2$ or $\mathrm{d}^2\Phi/\mathrm{d}T^2$, do coincide with the critical point for our PNJL model in the absence diquarks (see lower panel of Fig. 5). This is a consequence of the divergences in these quantities at the critical point. However, when including diquarks, a coincidence of critical point and crossover transition line is not guaranteed.

One finds that the critical endpoint depends sensitively on the degrees of freedom involved. From its position in the restricted NJL case (see also [17]) this point is shifted to higher $T$ by both, the effective Polyakov loop potential, and by the presence of diquark degrees of freedom. Near the critical endpoint not including diquarks, $\frac{\mathrm{d}\sigma}{\mathrm{d}T}$ diverges together with the chiral susceptibility. This extreme behaviour is not observed in the case with inclusion of diquarks. The region where this critical behaviour would appear is now already located in the diquark dominated phase.

Thus there is a qualitative difference of the critical endpoints in these two compared cases: not including diquarks the critical endpoint lies on top of the merging chiral and deconfinement crossover transition lines, while in the case including diquarks the critical endpoint is shifted away from this line. The critical endpoint now lies on the second order transition line bordering the diquark dominated phase (see lower panel of Fig. 5). I. e. the endpoint is not at the junction of all three transition lines and therefore is not a tri-critical point but still a critical point.

Next we use the PNJL model including diquark degrees of freedom to study the dependence of the position of the critical endpoint on the bare (current) quark mass. The upper right panel of Fig. 5 shows phase diagrams in the chiral limit, for current quark masses $m_0 = 5.5\,\mathrm{MeV}$ and $m_0 = 50\,\mathrm{MeV}$. The change of the critical endpoint with varying quark mass mainly reflects the dependence of the critical chemical potential on the quark mass. The presence of the diquark dominated phase appears to stabilize the temperature of the critical endpoint at rather high values.

Generally, the PNJL model generates the critical endpoint at a temperature which is significantly higher than the one found with the standard NJL model, i. e. ignoring Polyakov loop dynamics. The reason is that the diquark phase as well as the chiral phase is stabilized by the confinement emulation via the effective Polyakov loop potential. The size of the gap $\Delta$ is strongly influenced by the Polyakov loop. The detailed dependence of the gap on the Polyakov loop is displayed in Fig. 6. The systematics of this effect becomes evident when the Polyakov loop is held at fixed values and varied. The gap resulting from this calculation is then compared to the gap in the PNJL model (with self-consistent determination of $\Phi$) and in the NJL model. The case where the Polyakov loop is fixed to $\Phi = 1$ (i. e. complete deconfinement) coincides with the NJL calculation.

The presence of the Polyakov loop restricts the phase space available for quarks in the vincinity of their Fermi surface where Cooper pair condensation takes place. Hence a larger temperature is effectively required to break the pairs. This is the

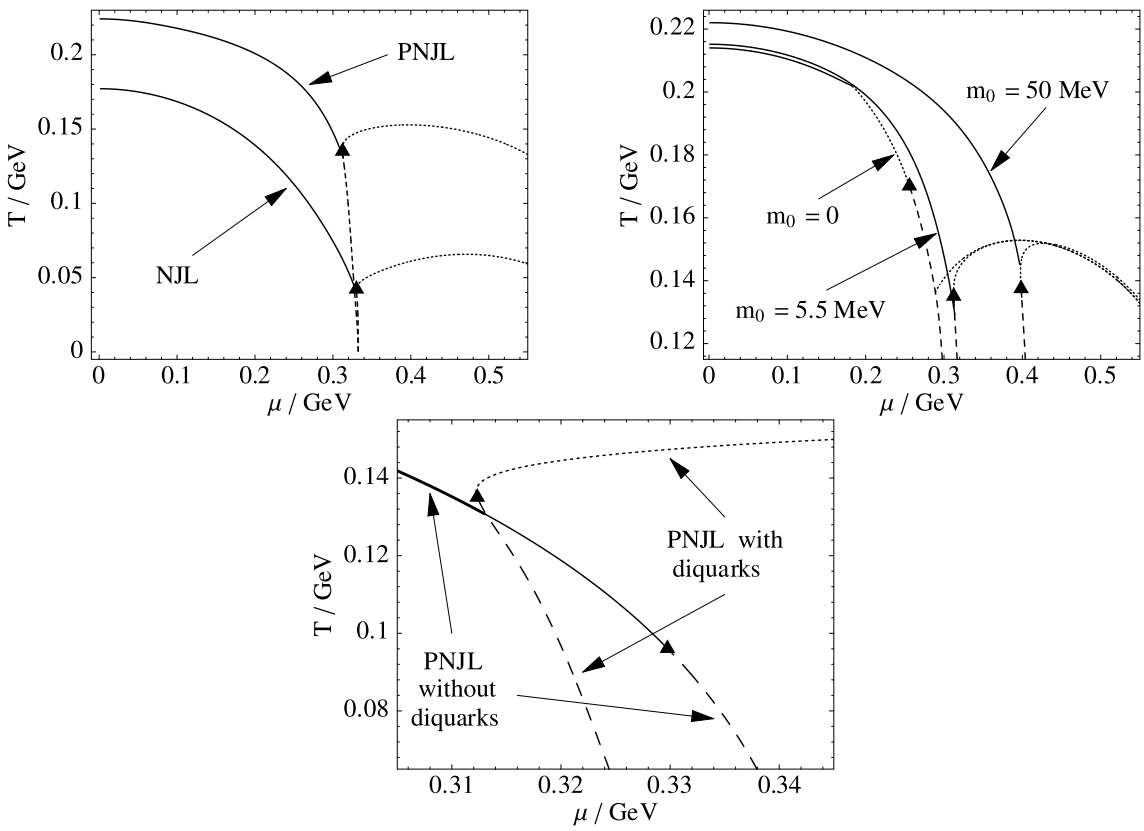


Figure 5: Upper left panel: comparison of the phase diagrams of NJL and PNJL model. The cross-over of the chiral condensate is drawn solid, first order lines are dashed and second order lines dotted. Upper right panel: comparison of the phase diagram at different current quark masses with inclusion of diquark degrees of freedom. (Note the scale on the temperature axis.) Lower panel: comparison of the PNJL model with and without inclusion of diquarks.

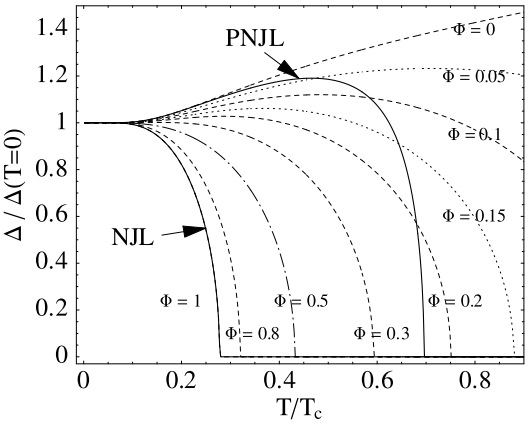


Figure 6: Dependence of the gap $\Delta$ on the presence of the Polyakov loop. The solid lines are the solutions to the self consistency equations of the NJL and the PNJL model at $T = 0.4\,\mathrm{GeV}$. The dashed lines are obtained by enforcing fixed values for the Polyakov loop. Note that the PNJL model with the Polyakov loop fixed at $\Phi = 1$ (deconfinement) coincides with the self consistent solution of the NJL model.

primary reason for the difference in behavior of the gap $\Delta$ when comparing NJL and PNJL results in Fig. 6.

## 3.3 Speed of sound

The velocity of sound $v_s$, determined by

$$v_s^2 = -\frac{1}{C_V}\frac{\partial\Omega}{\partial T}\bigg|_V \tag{17}$$

with the specific heat $C_V = -T(\partial^2\Omega/\partial T^2)_V$, shows a pronounced dip near the chiral and the deconfinement transition. This local minimum of the speed of sound becomes deeper in the vicinity of the critical endpoint of the first order phase transition line, separating the chiral phase at low chemical potential ($\mu \lesssim 1.5\,T_c$) from the diquark phase at high chemical potential ($\mu \gtrsim 1.5\,T_c$). When neglecting diquark degrees of freedom the speed of sound vanishes at the critical endpoint (solid curve in the central panel of Fig. 7).

Correspondingly, the specific heat diverges at this point. When diquark degrees of freedom are included in the calculation the critical endpoint is shifted such that the region of vanishing speed of sound would already be placed within the diquark dominated phase. This is why a vanishing speed of sound is not observed in the model including explicitly diquark degrees freedom (dashed curve in the central panel of Fig. 7). The discontinuity at higher temperatures is generated by the second order phase transition separating the diquark dominated phase from the high temperature

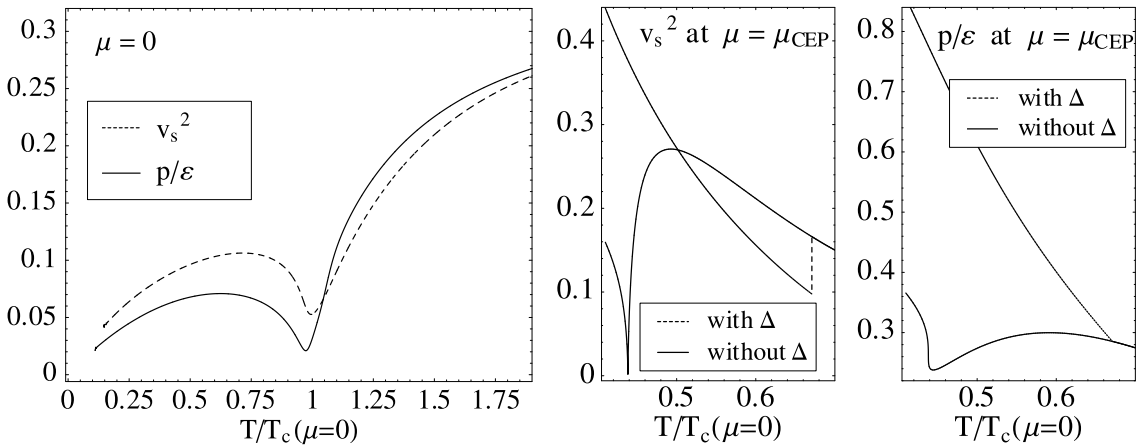


Figure 7: Left panel: Squared speed of sound (dashed) and ratio $\frac{p}{\varepsilon}$ (solid), and their dependence on the temperature at vanishing chemical potential. The two panels to the right: Studies of the sound velocity in the vincinity of the critical endpoint in the PNJL model without diquarks (at chemical potential $\mu = \mu_{\rm CEP}$). The PNJL model without diquarks is drawn with solid lines, the PNJL model with diquarks with dashed lines. Center panel: square of the velocity of sound. Right panel: pressure over energy density $\frac{p}{\varepsilon}$.

phase. Above this transition the two versions of the PNJL model (with and without explicit diquarks) become equivalent.

# 4 Concluding remarks and outlook

We have pointed out that an updated version of the PNJL model over and beyond the one used in [11, 16] leads to significantly better agreement with lattice data [4, 7], especially when extrapolating to finite chemical potential $\mu$. The combination of only two principal ingredients: chiral symmetry restoration and an effective potential ansatz for the confinement order parameter, appears to be sufficient to reproduce the available full QCD lattice computations to an astonishingly high accuracy, at least for temperatures $T$ up to about $2T_c$. The improvements shown in this paper in comparison with previous results [11, 16] originate in a better representation of the Polyakov loop part of the PNJL model. Taking into account the proper SU(3) constraints is crucial for an effective description of the thermodynamical implications of confinement.

Incorporating explicit diquark degrees of freedom influences the position and the nature of the critical endpoint in the $(T, \mu)$ phase diagram. The critical endpoint in the presence of diquarks is the connecting point between the chiral crossover transition line and the second order transition bordering the diquark dominated phase, while in the absence of diquarks it is the junction point of the chiral and decon-

finement crossover transition. The critical point in the PNJL-model with diquarks turns out not to coincide with the critical (diverging) behaviour of susceptibilities related to the chiral condensate and the Polyakov loop.

Further developments now aim for an extension of the present framework to $N_f = 3$ in order to explore the rich structure of colour superconducting (diquark) phases with three quark flavours and the additional effects of Polyakov loop dynamics.

# References


[1] P. de Forcrand and O. Philipsen, Nucl. Phys. B **642**, 290 (2002); Nucl. Phys. B **673**, 170 (2003).

[2] Z. Fodor and S. D. Katz, JHEP **0203**, 014 (2002); Z. Fodor, S. D. Katz, and K. K. Szabo, Phys. Lett. B **568**, 73 (2003).

[3] C. R. Allton *et al.*, Phys. Rev. D **66**, 074507 (2002); Phys. Rev. D **68**, 014507 (2003).

[4] C. R. Allton *et al.*, Phys. Rev. D **71**, 054508 (2005).

[5] G. Boyd *et al.*, Nucl. Phys. B **469**, 419 (1996).

[6] O. Kaczmarek, F. Karsch, P. Petreczky, and F. Zantow, Phys. Lett. B **543**, 41 (2002).

[7] O. Kaczmarek and F. Zantow, Phys. Rev. D **71**, 114510 (2005).

[8] G. Boyd, S. Gupta, F. Karsch, E. Laermann, B. Petersson and K. Redlich, Phys. Lett. B **349** (1995) 170, arXiv:hep-lat/9501029.

[9] K. Fukushima, Phys. Lett. B **591**, 277 (2004).

[10] P. N. Meisinger and M. C. Ogilvie, Nucl. Phys. Proc. Suppl. **47** (1996) 519, arXiv:hep-lat/9509050; Phys. Lett. B **379** (1996) 163, arXiv:hep-lat/9512011.

[11] C. Ratti, M. A. Thaler and W. Weise, Phys. Rev. D **73** 014019 (2006);
C. Ratti, M. A. Thaler and W. Weise, nucl-th/0604025.

[12] C. Ratti, S. Rößner, M. A. Thaler and W. Weise, Eur. Phys. J. C (2006), in print, arXiv:hep-ph/0609218.

[13] A. Dumitru, R. D. Pisarski and D. Zschiesche, Phys. Rev. D **72**, 065008 (2005).

[14] S. Rößner, Diploma Thesis, Technical University of Munich (2006).

[15] S. Rößner, C. Ratti, W. Weise, in preparation.

[16] S. K. Ghosh, T. K. Mukherjee, M. G. Mustafa and R. Ray, Phys. Rev. D **73** (2006) 114007.

[17] M. Buballa, Phys. Reports **407** (2005) 205.